

<https://doi.org/10.1038/s42004-024-01297-x>

# Direct glycosylation analysis of intact monoclonal antibodies combining ESI MS of glycoforms and MALDI-in source decay MS of glycan fragments

Check for updates

Isabella Senini<sup>1,2</sup>, Sara Tengattini<sup>1</sup>, Francesca Rinaldi<sup>1</sup>, Gabriella Massolini<sup>1</sup>, Christoph Gstöttner<sup>1,2</sup>, Dietmar Reusch<sup>3</sup>, Marcello Donini<sup>4</sup>, Carla Marusic<sup>4</sup>, Peter A. van Veelen<sup>1,2</sup>, Elena Domínguez-Vega<sup>1,2</sup>, Manfred Wuhrer<sup>1,2</sup>, Caterina Temporini<sup>1</sup> & Simone Nicolardi<sup>1,2</sup>✉

Monoclonal antibody (mAb) glycoengineering has the potential to improve the efficacy of biopharmaceuticals by fine-tuning specific biological properties. Glycosylation analysis is key to monitoring the glycoengineering process. Various mass spectrometry (MS)-based methods are available to characterize mAb glycosylation at different structural levels, but comprehensive analysis is typically time-consuming and costly. Here, we present an approach that combines conventional intact mass measurement of glycoforms by direct infusion ESI-MS with an advanced MALDI-in-source decay FT-ICR MS method for direct analysis of glycans in intact mAbs, without the need for enzymatic release and separation. Using a sodium-doped MALDI matrix, glycans were directly released as ISD fragment ions from the intact mAbs during the ionization process. Measurement of  $^{0,2}A$  fragment signals yielded reproducible glycan profiles that were consistent with conventional methods, yet was achieved with unprecedented speed, providing complementary information to that obtained through intact mass measurement. The methods were applied to standard and glycoengineered trastuzumab and rituximab, allowing rapid glycosylation profiling and structural analysis of glycans by tandem MS of selected ISD fragment ions. This fast approach can facilitate the early-phase development of glycoengineering processes by constraining further in-depth analyses. We envision a broader applicability in studies focused on glycosylation changes in mAbs.

Recent advancements in biotechnology and genetic engineering have enabled the development of novel biopharmaceutical proteins with specific glycosylation traits<sup>1</sup>. Glycosylation plays a key role in determining the structure, function, and stability of proteins therefore, pharmaceutical proteins, such as therapeutic monoclonal antibodies (mAbs), can be glycoengineered to improve their biological properties<sup>2–4</sup>. Glycosylation of the Fc domain in mAbs impacts immune effector functions such as antibody-dependent cell-mediated cytotoxicity (ADCC) and complement-dependent cytotoxicity (CDC)<sup>5</sup>. These mechanisms are critical in determining the efficacy of IgG-based therapeutic mAbs<sup>6–9</sup>. Many therapeutic mAbs are expressed in mammalian cells such as Chinese hamster ovary (CHO) cells<sup>10</sup>.

Plant-based recombinant expression systems have been developed as a safe, cost-effective, and scalable alternative to mammalian cell cultures<sup>11–13</sup>. Beyond mammalian cells and plants, other expression systems include bacteria, yeasts, fungi, and insect cell lines<sup>14</sup>. To refine the glycosylation profile of in vivo-produced mAbs, chemoenzymatic treatments involving enzymes like endoglycosidases and glycosynthases are employed<sup>15</sup>. These treatments aim to obtain mAbs with well-defined and consistent glycan structures, ultimately reducing batch-to-batch variability.

The development and optimization of glycoengineering processes depend on a series of glycosylation analyses designed to assess the effectiveness of in vivo or in vitro engineering experiments. Various

<sup>1</sup>University of Pavia, via Taramelli 12, Pavia, Italy. <sup>2</sup>Leiden University Medical Center, Albinusdreef 2, Leiden, The Netherlands. <sup>3</sup>Pharma Technical Development Penzberg, Roche Diagnostics GmbH, Penzberg, Germany. <sup>4</sup>Laboratory of Biotechnology, ENEA Casaccia Research Center, Via Anguillarese 301, Roma, Italy.

✉ e-mail: [s.nicolardi@lumc.nl](mailto:s.nicolardi@lumc.nl)

methodologies are available for glycoprotein analysis, each offering unique structural insights<sup>16,17</sup>. Mass spectrometry (MS) is a versatile tool for characterizing glycoproteins at different structural levels<sup>18–20</sup>. It enables the analysis of intact proteins, subunits, glycopeptides, and released (N-)glycans, allowing for a comprehensive determination of macro and micro-heterogeneity of post-translational modifications. However, achieving an in-depth characterization often requires a multi-methods approach, which can be both time-consuming and costly. Therefore, there is a need for rapid and direct glycosylation analysis, providing sufficient information to instruct decision-making. Over the last decade, top-down MS strategies for the characterization of mAbs have made significant progress<sup>18,21–25</sup>. These strategies allow for intact mass measurement which is typically performed at low mass resolution and provides direct and unique information on the combinatory presence of glycans on different mAb subunits<sup>26</sup>. However, glycan abundance cannot typically be directly derived from the glycosylation profile determined at the intact protein level. This is because the pairing of subunits carrying different glycans is not stochastic, some combinations result in isomeric structures indistinguishable by MS, and even glycoforms with similar masses are not distinguishable. Furthermore, the presence of other protein modifications, such as methionine oxidation, N-terminal glutamine (Q)/glutamic acid (E) to pyroglutamate (pyroGlu) conversion, deamidation, and terminal clipping, can affect the interpretation of glycoform profiles when proteoforms resulting from these modifications are not separated prior to analysis. Although top-down MS/MS analysis of intact mAbs can provide information on the glycosylation site of major glycoforms, further characterization of glycans by MS<sup>n</sup> of glycosylated fragment ions is typically limited.

In this context, we have developed a direct MALDI-ISD FT-ICR MS approach that complements intact mass measurement of mAbs, providing a tool to accelerate the glycoengineering development process by quickly generating glycan profiles with unambiguous compositional information, thanks to the use of accurate mass measurements, and with the advantage of obtaining structural insights via tandem MS.

Matrix-assisted laser desorption/ionization (MALDI) MS allows for rapid analysis of glycoproteins at different structural levels<sup>18,27–29</sup>. This technique offers several advantages, including fast data generation, straightforward results, excellent analyte selectivity, minimal carryover, and the potential for high-throughput and automated sample processing. When combined with in-source decay (ISD) fragmentation, MALDI MS becomes a powerful tool for quickly characterizing the terminal amino acid sequences of mAbs<sup>18,23,30–32</sup>. By using specific MALDI matrices like 1,5-diaminonaphthalene (1,5-DAN) or 2,5-dihydroxybenzoic acid (DHB) and specific laser conditions, the peptide backbone of intact proteins undergoes fragmentation directly during the ionization process<sup>33–35</sup>. The simultaneous mass analysis of all generated fragment ions leads to mass spectra rich in information. Fragmentation of selected ISD fragment ions by tandem MS further extends the structural insights.

Furthermore, the use of ultrahigh-resolution MS, such as Fourier-transform ion cyclotron resonance (FT-ICR) MS, maximizes structural information and enhances result confidence<sup>36–38</sup>. While applications of MALDI-ISD MS for the analysis of protein sequences are well-documented in the literature, the direct analysis of glycans from intact glycoproteins without enzymatic release is a recent development. Urakami and Hinou employed this approach to analyze N-glycans from model glycoproteins like ribonuclease B (RNase B), ovomucoid, and egg white<sup>39,40</sup>. Our group applied this direct method for the analysis of O-antigen polysaccharides in bioengineered glycoconjugate bacterial vaccines<sup>41</sup>. The presence of sodium in the MALDI matrix was crucial for selectively detecting glycan fragments over protein fragments.

In this study, we demonstrate the effectiveness of MALDI-ISD FT-ICR MS for the analysis of glycans directly from intact mAbs. We aimed to demonstrate the utility of this approach, combined with intact mass measurement, in evaluating the success of glycoengineering processes. To achieve this, we analyzed a series of standard mAbs and their glycoengineered counterparts, including SiLu™ Lite MSQC4 standard (SiLuLite mAb),

trastuzumab, and rituximab. SiLuLite mAb is commonly used as a standard for method development and validation, while trastuzumab and rituximab are therapeutic proteins targeting receptor tyrosine-protein kinase erbB-2 (HER2) and the B-lymphocyte antigen CD20, respectively<sup>42,43</sup>. Trastuzumab is used to treat breast and stomach cancers, whereas rituximab is used for non-Hodgkin lymphoma, chronic lymphocytic leukemia, and certain autoimmune diseases such as rheumatoid arthritis. These three mAbs are glycosylated in the fragment crystallizable region with the main glycans being Man5, G0, G1, G0F, G1F, and G2F (see Fig. S1 for corresponding glycan structures).

Our results show that glycosylation profiles can be obtained with high repeatability and accuracy, facilitating the identification of glycosylation differences between standard and glycoengineered mAbs. Furthermore, an advantage of this approach is that the generation of glycan fragments directly from intact mAbs allows for the corroboration of their monosaccharide composition by subsequent tandem MS analysis. This method is not only rapid but also eliminates the need for enzymatic N-glycan release, offering direct access to glycosylation information, thereby enhancing efficiency and eventually accelerating decision-making in the development process.

## Results

### Direct glycosylation analysis from SiLuLite mAb by MALDI-ISD FT-ICR MS

We established a workflow for the direct glycosylation analysis of intact glycoengineered mAbs combining intact mass measurement by ESI FT-ICR MS and direct glycan analysis by MALDI-ISD FT-ICR MS (Fig. 1). Initially, we optimized and validated the workflow with the standard mAb SiLu™ Lite MSQC4 (SiLuLite mAb) (Fig. 2). This mAb, produced in CHO cells, exhibited core fucosylated G0F, G1F, and G2F, as well as afucosylated G0, G1, and Man5 glycan structures as determined by LC-MS analyses of glycopeptides by Srzentić K and coworkers<sup>18</sup>, and us (see Figs. S1 and S7).

Intact mass measurement revealed the presence of five major mAb glycoforms, namely G0/G0F, G0F/G0F, G0F/G1F, G1F/G1F isomeric with G0F/G2F, and G1F/G2F (Fig. 2b) while some minor species were identified as phosphate adducts.

Direct glycan analysis by MALDI-ISD FT-ICR MS, using optimized MALDI conditions, allowed us to detect glycan fragments directly from the intact mAb without the need for an enzymatic release (Fig. 2c). The use of sodium in the MALDI matrix suppressed protein fragmentation enhancing the detection of glycans (see Fig. S2). These were mainly detected as cross-ring <sup>02</sup>A and <sup>24</sup>A fragments that were generated from cleavage at the innermost, peptide-linked GlcNAc residue (see Fig. S1). Notably, while the <sup>02</sup>A fragments of core-fucosylated glycans maintained the core fucose, <sup>24</sup>A fragmentation resulted in the loss of the  $\alpha$ 1,6-linked fucose residue, leading to afucosylated <sup>24</sup>A fragments. For example, the fragmentation of G1F and G1 glycans led to the formation of identical <sup>24</sup>A fragments (detected at  $m/z$  1340.4601). Consequently, solely the signal of diagnostic <sup>02</sup>A fragments of the different glycans was used to generate a glycan profile that was in good agreement with data obtained by glycopeptide analysis (Figs. 2d and S7), with relative standard deviation varying from 2.4% to 9.8%.

Loss of core GlcNAc with the formation of relatively intense B ions was also observed (e.g. fragments at  $m/z$  1280.4387 and  $m/z$  1118.3864) as well as the combination of core and branch cleavages that led to a more extensive fragmentation of the main glycan structures (e.g. <sup>24</sup>AY at  $m/z$  975.3273, <sup>02</sup>AY ion at  $m/z$  1035.3484 and BY ion at  $m/z$  1077.3595).

Despite the presence of a chemical background noise derived from MALDI matrix cluster ions, protein fragments, and matrix adducts, mass measurements at high resolving power (208,000 at  $m/z$  975.3273 and 109,000 at  $m/z$  1708.5908) and the distinct mass defect of glycan ions enabled the confident identification of the glycan fragments (see Supplementary Notes: *Evaluation of protein fragment ions and matrix adducts*). For simplicity, solely glycan fragments are indicated in the figures.

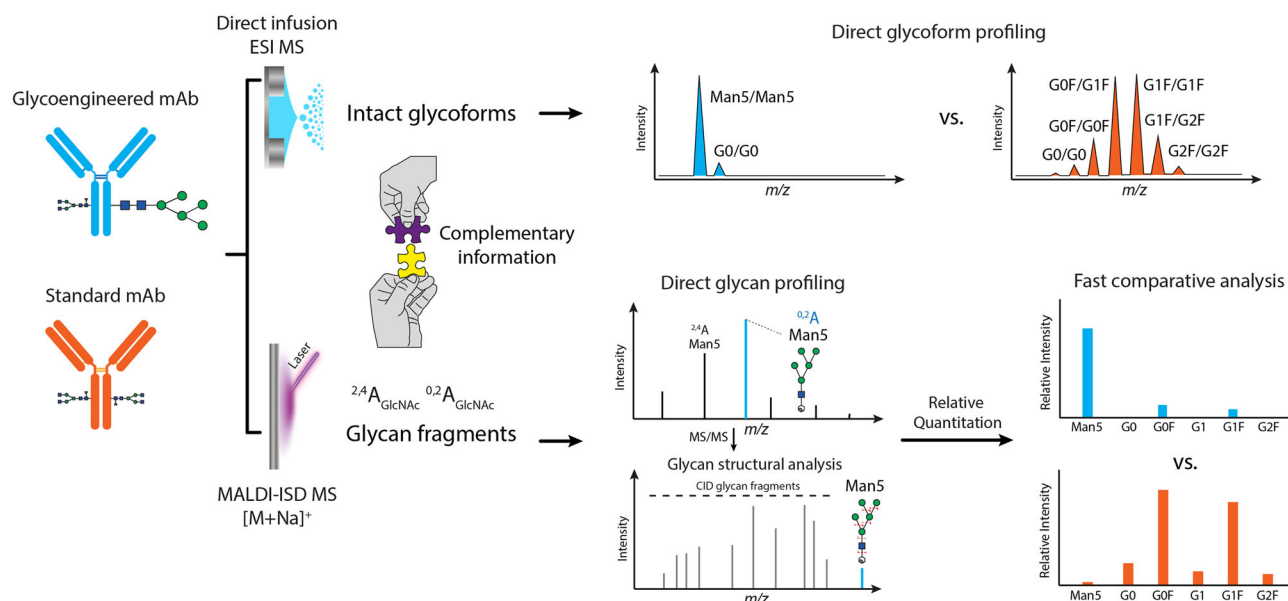


**Fig. 1 | Workflow for direct glycosylation analysis from intact standard and glycoengineered mAbs by ESI MS and MALDI-ISD MS.** Glycosylation of mAb is characterized at intact protein level using direct infusion ESI MS and at glycan level using a newly developed MALDI-ISD MS method. The latter analysis eliminates the need for glycan release. In fact, under the applied MALDI conditions, ISD fragmentation specifically targets the core GlcNAc residue attached to the Fc

portion, predominantly generating  $^{24}A$  and  $^{0,2}A$  glycan fragments. The detection of these glycan fragments facilitates the direct profiling of the major glycan species in both standard and glycoengineered mAbs. Subsequently, the glycan of interest can be structurally characterized through MS/MS. The two methods provide complementary structural information in a fast manner. Glycan residue symbols: blue square, N-acetylglucosamine; green circle, mannose; red triangle, fucose.

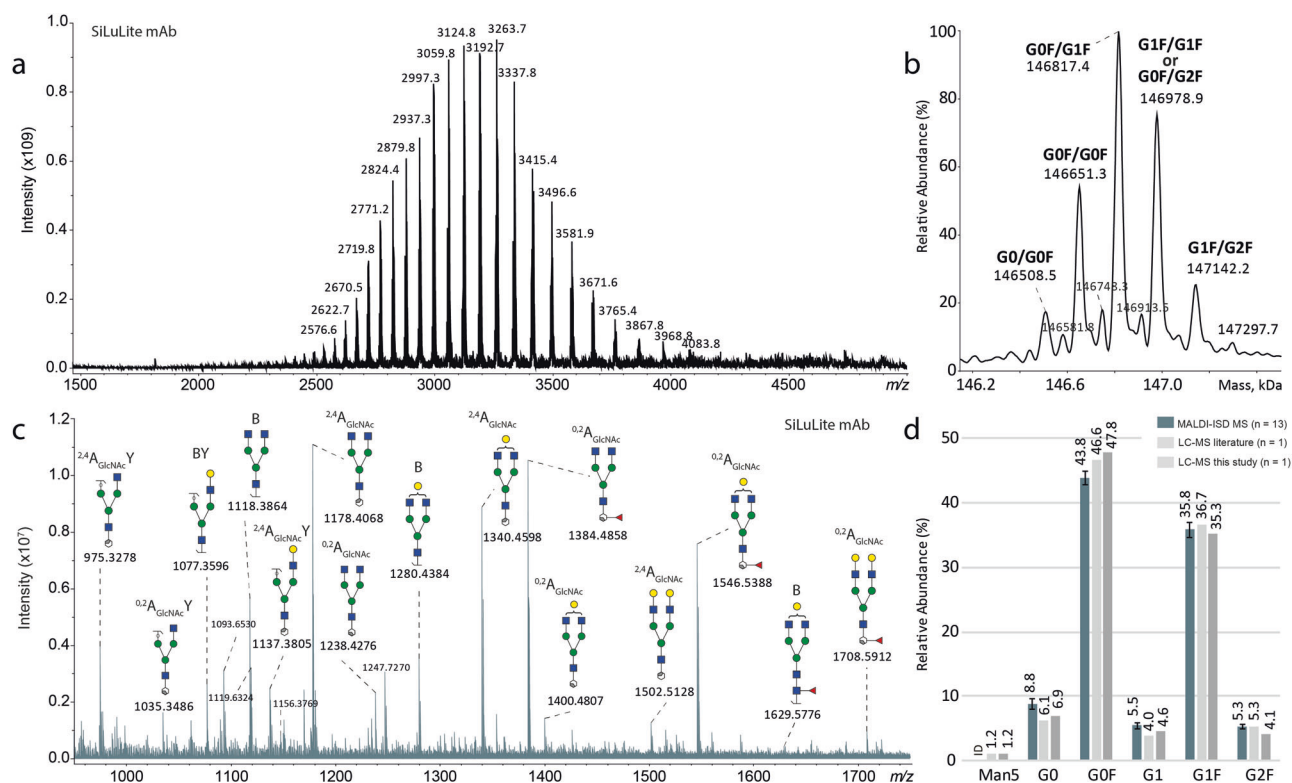


**Fig. 2 | Direct glycosylation analysis from intact SiLu™ Lite MSQC4 mAb expressed in CHO cells.** **a** Direct infusion ESI FT-ICR mass spectrum of SiLu™ Lite MSQC4. **b** Maximum entropy deconvolved ESI FT-ICR mass spectrum of SiLu™ Lite MSQC4. Five major mAb glycoforms were detected. Some minor species were associated with phosphate adducts. **c** MALDI-ISD FT-ICR mass spectrum of SiLu™ Lite MSQC4. Solely glycan fragments are indicated (see Supplementary Notes:

*Evaluation of protein fragment ions and matrix adducts).* **d** Glycosylation profiles obtained by MALDI-ISD MS considering  $^{0,2}A$  fragments and two glycopeptide analyses by LC-MS (see Fig. S7).<sup>18</sup> ID = Inconsistently detected. Glycan residue symbols: blue square, N-acetylglucosamine; green circle, mannose; yellow circle, galactose; red triangle, fucose.

### Direct glycosylation analysis from standard and glycoengineered mAbs

The workflow developed for the analysis of SiLuLite mAb was applied to both standard trastuzumab and a glycoengineered variant produced in CHO cells treated with kifunensine and subjected to trimming with  $\alpha$ 1,2-mannosidase (Fig. 3). The primary glycan structures on standard trastuzumab included G0, G1, G0F, G1F, and G2F and, to a minor extent, G0-GlcNAc and G1-GlcNAc, as determined by 2AB-labeling of released N-glycans with LC-fluorescence detection (FD) and LC-MS analyses of glycopeptides (see Figs. S8, S9 and S10). In contrast, the glycoengineered variant exhibited Man5, Man4, G0F, and G1F glycan structures. ESI MS analysis allowed for the rapid determination of the glycosylation differences at the intact protein level. The glycoforms Man5/Man5, G0/G0, G0/G0F, G0F/G0F, G1F/G1F (or G0F/G2F), G1F/G2F, G2F/G2F and G1FS/G2F (or G2FS) were identified for standard trastuzumab while the glycoforms Man5/Man5, and G0/G0 were identified for trastuzumab Man5 (Fig. 3a, b and S11).

MALDI-ISD MS analysis enabled the rapid determination of glycosylation differences at the glycan level, directly from the acquired mass spectra (Fig. 3c, e) and derived glycan profiles (Fig. 3d, f). The glycan profiles showed relative intensities varying from 2.8% to 10.6% for standard trastuzumab and from 1% to 9.9% for trastuzumab Man5. G0/G0F-GlcNAc and G1-GlcNAc structures of mAbs could not be distinguished from those generated from the loss of a GlcNAc residue during the ionization process, as seen in SiLuLite mAb mass spectra, and therefore were not included in the evaluation.

Standard rituximab and a glycoengineered variant expressed in tobacco were also analyzed (Fig. 4). The glycosylation of standard rituximab, expressed in CHO cells, was similar to SiLuLite mAb while the variant solely exhibited G0 (Figs. S1, S12 and S13). Intact protein analysis by ESI MS revealed the glycoforms G0/G0, G0/G0F, G0F/G0F, G0F/G1F, G1F/G1F (or G0F/G2F) for standard rituximab while only the glycoform G0/G0 and two G0/G0 proteoforms, derived from the presence of the terminal lysine on either only one or both of the two heavy chains of the mAb, were detected (Fig. 4a, b). The presence of terminal lysine was corroborated in the LC-MS data (see Fig. S14).

Glycosylation differences between standard rituximab and its plant-derived variant, directly observable in MALDI-ISD mass spectra (Fig. 4c, e), were summarized in the derived glycan profiles obtained from the measurement of  $^{0,2}A$  fragments (Fig. 4d, f). These showed relative standard deviation varying from 1.4% to 9.7%. Of note, protein fragments of rituximab were detected at a higher intensity than those of SiLuLite mAb and trastuzumab mAbs (Fig. S4). Another rituximab variant expressed in tobacco and exhibiting oligomannose glycans was also characterized using our workflow. Unfortunately, due to the low amount available, solely MALDI-ISD MS analysis was successful in providing glycosylation information at the glycan level (see Figs. S15 and S16).

### Structural analysis of glycan fragment ions by MS/MS

Sodiated glycan fragments generated by MALDI-ISD were further characterized by collision-induced dissociation (CID) (Fig. 5 and S17). Although solely the signal of  $^{0,2}A$  fragments was used to generate the derived glycan

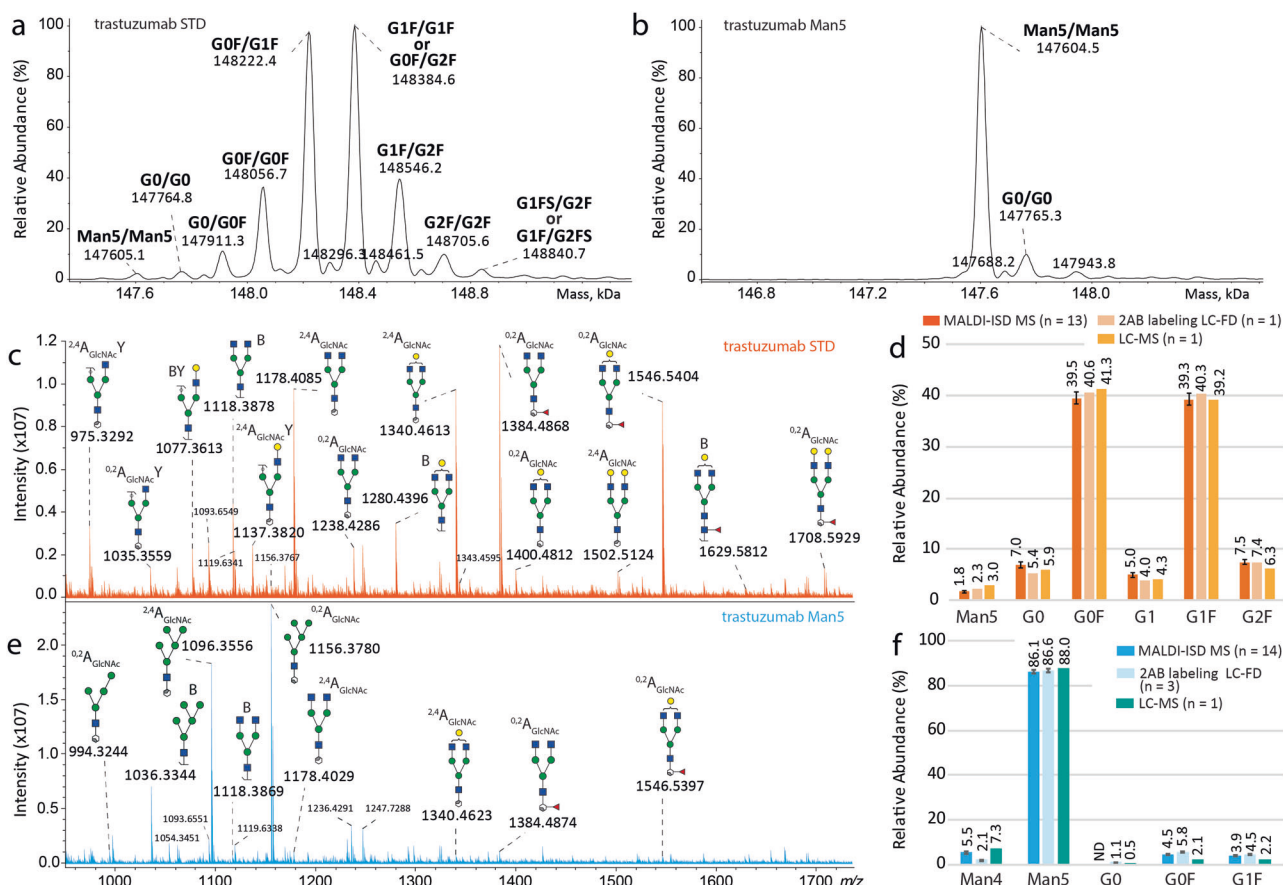


**Fig. 3 | Direct glycosylation analysis from intact standard and glycoengineered trastuzumab mAbs expressed in CHO cells.** Maximum entropy deconvolved ESI FT-ICR mass spectra of (a) standard and (b) glycoengineered trastuzumab (raw mass spectra are reported in Fig. S11). MALDI-ISD FT-ICR mass spectrum of (c) standard and (e) glycoengineered trastuzumab. Glycosylation profiles of (d) standard and (f) glycoengineered trastuzumab obtained by MALDI-ISD MS considering

$^{0,2}A$  fragment ions, 2AB labeling LC-FD analysis and LC-MS (Figures S8–10). Solely glycan fragments are indicated in the mass spectra (see Supplementary Notes: *Evaluation of protein fragment ions and matrix adducts*). Glycan residue symbols: blue square, N-acetylglucosamine; green circle, mannose; yellow circle, galactose; red triangle, fucose.

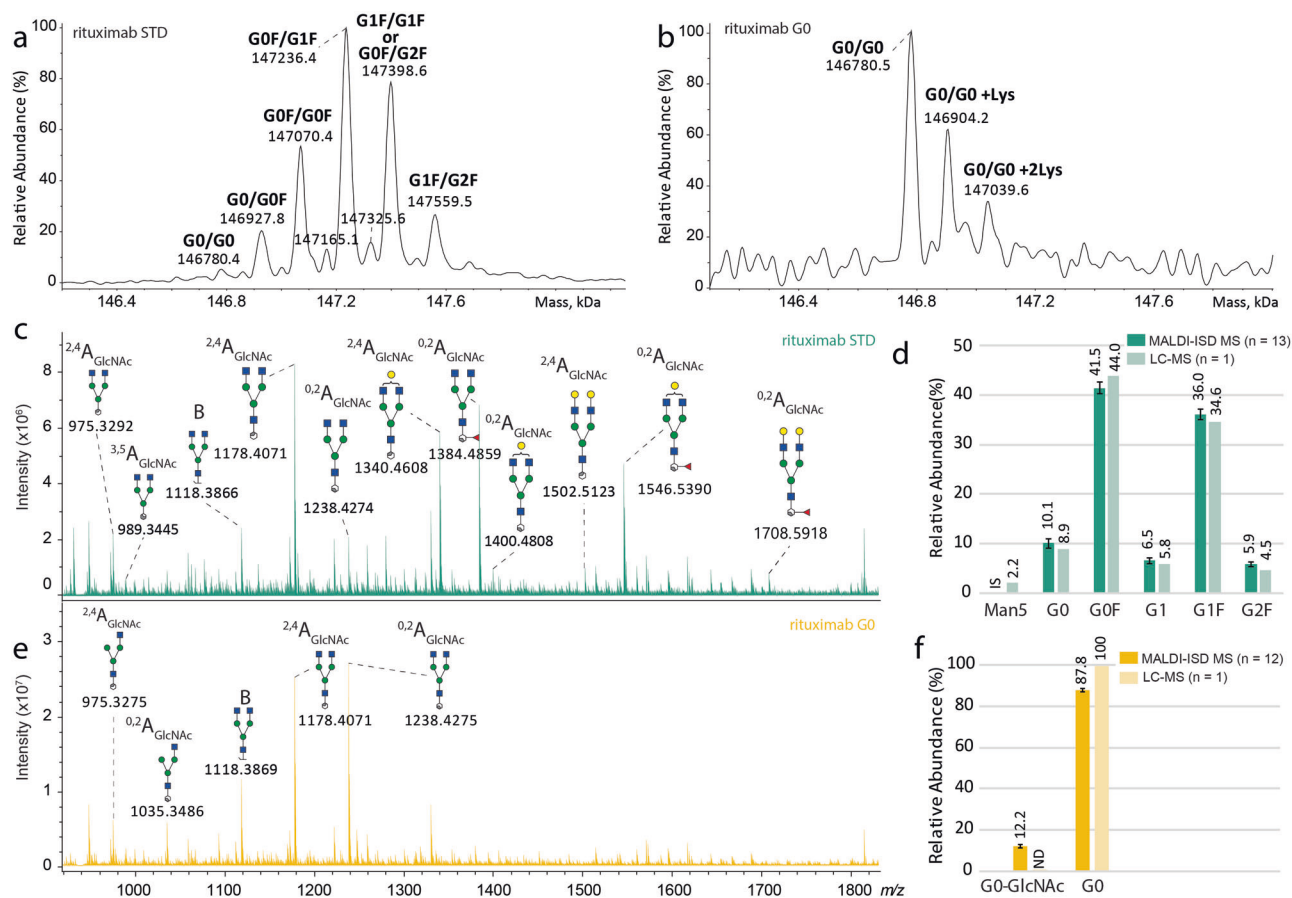


**Fig. 4 | Direct glycosylation analysis from intact standard and glycoengineered rituximab mAbs.** Maximum entropy deconvolved ESI FT-ICR mass spectra of (a) standard and (b) glycoengineered rituximab (raw mass spectra are reported in Fig. S12). MALDI FT-ICR MS mass spectra of (c) rituximab STD from CHO cells and (e) rituximab G0 glycoengineered variant produced in plants. Glycosylation profiles of (d) rituximab STD, and (f) rituximab G0 glycoengineered variant

obtained by MALDI-ISD MS considering  $^{0,2}A$  fragments and LC-MS glycopeptide analysis (Fig. S13). Solely glycan fragments are indicated in the mass spectra (see Supplementary Notes: *Evaluation of protein fragment ions and matrix adducts*). ID = Inconsistently Detected. ND = not detected. Glycan residue symbols: blue square, N-acetylglucosamine; green circle, mannose; yellow circle, galactose; red triangle, fucose.

profiles, both  $^{0,2}A$  and  $^{2,4}A$  types were analyzed by CID. The obtained structural information allowed us to further corroborate the glycan composition (i.e. as number of hexose, N-acetylhexosamine, and fucose residues). Typically, the most intense CID fragment ions were generated from the cleavage of glycosidic bonds while cross-ring fragments were detected to a minor extent. Some fragments derived from multiple glycosidic cleavages, for example, the Hex3 fragment at  $m/z$  509.1479 of  $^{0,2}A$ -G1F (Fig. 5c). Isomeric fragment structures could not be distinguished therefore, and fragments were assigned with a likely cleavage type and the monosaccharide composition (Fig. S18).

## Discussion

Glycosylation analysis is crucial for the development of glycoengineered mAbs. Detailed determination of macro- and micro-heterogeneity of such complex molecules requires the use of a multi-methods approach that includes both simple and complex analyses. In this study, we aimed to obtain glycosylation information from intact mAbs by combining two direct methods: the well-established intact protein analysis via direct infusion ESI MS, and a new approach for direct glycan analysis based on MALDI-ISD MS.

Intact protein analysis without any separation may be considered the simplest MS-based analysis that provides glycosylation information at a macro level. Applied to mAbs, it is typically performed at low mass resolution and suffers from a low sensitivity for low abundant glycoforms. For example, the low-abundant glycoform Man5/Man5 was not detected in the intact mass measurements of SiLuLite mAb and standard rituximab

(Figs. 2b and 4a). Notably, in a recent study on the characterization of SiLuLite mAb, this glycoform could only be detected after averaging data from multiple LC-MS replicate analyses performed on an Orbitrap FTMS system, indicating that the detection of Man5/Man5 is not trivial<sup>18</sup>. The combination of heterogeneous mAb subunits can lead to isomeric glycoforms which cannot be distinguished in the intact protein analysis. For example, the isomeric glycoforms G1F/G1F and G0F/G2F (see Figs. 2b, 3a and 4a) were detected as a single peak. Even glycoforms with small mass differences cannot be discriminated. In fact, glycoforms carrying G1 were not detected in any of the mAbs carrying it. The presence of interfering ion species such as adducts with residual buffer components or protein modifications different than glycosylation increases the mass spectra complexity further hampering interpretation. For example, adducts with residual phosphate ions were observed for SiLuLite mAb while proteoforms with residual C-terminal lysine on the heavy chains were found in rituximab G0 (Fig. 4b). As a result of these limitations, a glycan profile could not be inferred from intact mass measurement since the contribution to the signal of each glycoform was not determinable. Nevertheless, intact protein analysis provided unique information on the combinatory presence of glycans on the different subunits of a mAb and could be used to determine major glycosylation differences between standard and glycoengineered mAbs.

Following recent developments on the direct analysis of glycans from intact glycoproteins using MALDI MS<sup>39–41</sup>, we developed a method for the direct analysis of glycans from intact mAbs that does not require any enzymatic treatment or separation technique, with MSMS capabilities, and that provides information on glycosylation micro-heterogeneity. By using a

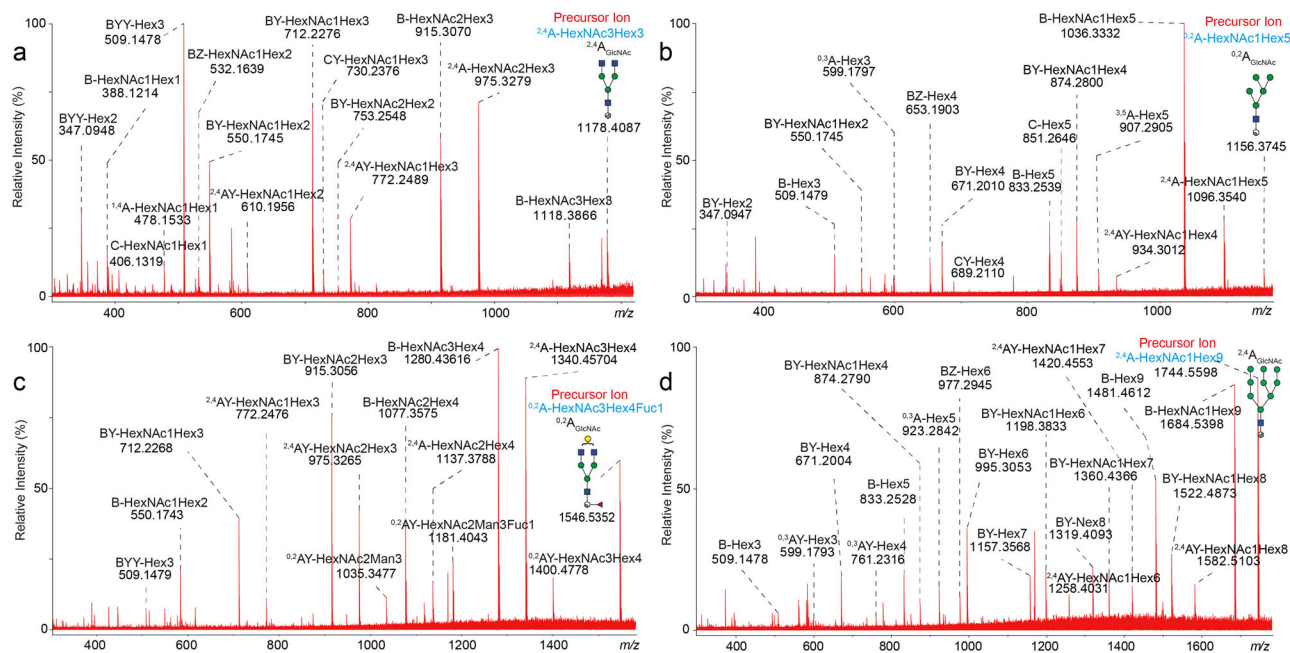


**Fig. 5 | MALDI-MS/MS CID FT-ICR mass spectra of glycan fragment ions.** Examples of CID tandem mass spectra obtained from the analysis of both  $^{2,4}A$  and  $^{0,2}A$  glycan fragments are provided: **a**,  $^{2,4}A_{\text{GlcNAc}}$  of G0 or G0F; **b**,  $^{0,2}A_{\text{GlcNAc}}$  of Man5; **c**,  $^{0,2}A_{\text{GlcNAc}}$  of G1F; and **d**,  $^{2,4}A_{\text{GlcNAc}}$  of Man9. More examples are reported in Fig. S17. Tentative

assignments are reported indicating the type of fragmentation and monosaccharide composition (Fig. S18). Glycan residue symbols: blue square, N-acetylglucosamine; green circle, mannose; yellow circle, galactose; red triangle, fucose.

MALDI matrix composed of DHB, 1,5-DAN and sodium bicarbonate, protein fragments were suppressed enhancing the detection of glycan fragments that were generated directly during the MALDI process. Among all detected glycan fragments, solely cross-ring  $^{0,2}A$  fragments were univocally diagnostic for the different glycan structures and allowed the generation of reproducible glycan profiles that well matched the glycosylation profiles obtained by other conventional methods. These profiles included glycan that could not be discriminated at intact protein level. For instance, G1 was consistently measured in all three mAb standards while Man5 was detected even in SiLuLite mAb and standard rituximab. The complementarity of the two direct methods is also shown in the results of trastuzumab Man5. In this mAb, the glycoform G0/G0 was detected with a relative intensity of about 10% while G0 was not detected in the glycan profiles obtained by MALDI-MS and was observed at a much lower level by 2AB labeling LC-FD and LC-MS analyses. Residual G0F and G1F, derived from a minor inefficiency of the kifunensine treatment, were instead detected in the MALDI-MS profiles but not at the intact protein level. The use of genome editing in tobacco plants was successfully used to knock out fucosyltransferase and xylosyltransferase genes to avoid plant-specific glycosylation and produced a glycoengineered variant of rituximab that contained primarily G0<sup>14</sup>. Intact mass measurements of rituximab G0 suffered from a low sensitivity due to a low concentration of the sample and the presence of residual C-terminal lysine on the heavy chains. Our method allowed us to assess the presence of the rituximab variant carrying G0 glycan only, confirming the effectiveness of this glycoengineered plant line and product homogeneity.

In the MALDI-MS analysis, glycans up to a relative intensity of about 2% were consistently detected in replicate measurements with reproducibility values suitable for the determination of large differences between standard and glycoengineered mAbs. Less abundant species (i.e. Man5 in SiLuLite mAb) may be detected in some replicate measurements but their signal suffers from low reproducibility.

Excessive ISD of the glycan structures was observed affecting the determination of the relative abundance of some endogenous glycans. For example, the loss of GlcNAc during ionization affected the signal of G0/G0F-GlcNAc and G1-GlcNAc to the point that these glycans were not

included in the evaluation. This resulted in an overestimation of the calculated relative intensity of the glycoforms that were included in the evaluation. Nevertheless, the obtained glycan profiles well described the glycosylation differences among samples providing useful information.

The study covers most of the glycan structures potentially present in therapeutic mAbs at high levels<sup>10</sup>. Typically, the MALDI analysis of sialylated glycans is hampered by in-source and metastable decay thus derivatization strategies are needed to stabilize sialic acid residues during the ionization<sup>45</sup>. Low-abundant glycoforms containing sialic acids were detected for standard trastuzumab by intact mass analysis but not by MALDI-MS. Preliminary results, not included in this study, show that the analysis of sialylated mAbs using our approach would require the implementation of a derivatization step. Since we aimed to develop a simple, fast and direct method, such derivatization strategies were not implemented and the analysis of sialylated mAbs was not included in the study.

MALDI-MS protein fragment ions are better detected as protonated ions rather than sodiated. Thus, the presence of sodium in the MALDI matrix resulted in the suppression of protein fragments. Typically, the MALDI-MS mass spectra of mAbs, obtained without sodium, include N- and C-terminal fragments from light and heavy chains while internal fragments are not detected<sup>23</sup>. The fragmentation pattern and signal intensity of these fragments are amino acid sequence-dependent, and we, therefore, expected differences in the level of suppression in the analysis of different mAbs. Accordingly, protein fragments were less suppressed for rituximab compared to other mAbs, showing some prominent sodiated internal protein fragments. The detection of protein fragments was not a limitation for the analysis of glycans since these two classes of molecules have different mass defects and the use of high-resolution MS allowed us to distinguish glycan from peptide fragments with high confidence.

The cleavage of the glycans from intact mAbs in the ionization source allowed us to perform MS/MS on selected precursor ions using CID providing additional insights into the glycan composition. This characterization option is an advantage compared to top-down analysis of intact mAb that, despite providing information on the glycosylation site, typically gives limited information on the glycans attached to the protein fragments. Instead, MALDI-MS CID MS provides molecular fingerprints that can be

used for the corroboration of the glycan structures of newly obtained glycoengineered mAbs. Furthermore, compared to the analysis of protonated species, the MS/MS characterization of sodiated glycans produces different fragmentation profiles. These profiles can offer complementary structural insights and do not exhibit monosaccharide rearrangement, such as fucose migration<sup>46</sup>.

## Conclusion

In this study, we propose a strategy for the direct glycosylation analysis of intact mAbs based on conventional intact glycoform analysis by direct infusion ESI FT-ICR MS and glycan analysis by MALDI-ISD FT-ICR MS. The two methods provide complementary structural information with the newly developed MALDI-ISD MS method providing direct access to glycan information and allowing a fast comparison between standard and glycoengineered mAbs directly from the easy-to-interpret mass spectra or derived glycan profiles without the need for time-consuming sample preparation, analyses, and data processing. The proposed method allows for targeted MSMS analysis which provides additional information on the monosaccharide composition of selected glycans.

Access to the high-end technology used in this study may be a prerogative of large biopharmaceutical companies. However, the implementation of this direct analytical strategy in technology-focused infrastructures can provide support to small- or medium-size biopharmaceutical industries and academic research groups. For example, the method could be used in screening strategies aimed to speed up the early-phase development of glycoengineering processes by limiting further in-depth analysis for example solely to mAb samples that are obtained from successful optimizations. Similarly, the method can facilitate research activities aimed at evaluating glycosylation changes of mAbs in biological experiments.

Finally, the implemented MALDI-ISD MS method expands the toolkit of top-down MS techniques for the characterization of mAbs giving access to glycan information in a fast manner, without the need for any enzymatic release or chromatographic separation.

## Methods

### Samples, material, and reagents

SiLu™ Lite MSQ4C4 universal antibody standard human expressed in CHO cells (SiLuLite mAb), SiLu™ Lite MSQC17 rituximab monoclonal antibody expressed in CHO cells (rituximab STD), 2,5-dihydroxybenzoic acid (DHB), 1,5-diaminonaphthalene (1,5-DAN) and ammonium bicarbonate were purchased from Sigma-Aldrich Corp. (St. Louis, MO, USA). Trastuzumab (trastuzumab STD) and glycoengineered trastuzumab (trastuzumab Man5) were provided by Roche (Basel, Switzerland). Two different glycoengineered rituximab forms obtained in genetically modified plants were supplied by ENEA Research Center (Rome, Italy), namely oligomannose rituximab and rituximab G0. Sodium bicarbonate (NaHCO<sub>3</sub>) was from Merck (Darmstadt, Germany). Acetonitrile (LC-MS grade) was purchased from Actua-All Chemicals B.V. (Oss, Netherlands) while water was obtained from an Elga LabWater Purelab Chorus Millipore system (Woodridge, IL, USA). Capture Select™ FcXL affinity matrix was supplied by Thermo Fisher (Waltham, MA, USA). Orochem filter plates were from Orochem Technologies Inc (Naperville, IL, USA) while conical-bottom 96 well-plates were purchased by Greiner Bio-One B.V. (Kremsmünster, Austria). Formic acid (FA) was supplied from VWR International (Radnor, PA, USA).

### Glycoengineered mAbs

Trastuzumab Man5 was produced by treating bioengineered CHO cells with kifunensine to produce an oligomannose mAb (Man9/8) that was purified and further treated with  $\alpha$ 1,2-mannosidase. Vacuum-agroinfiltration of plants was performed as described by Tengattini and colleagues and enabled transient antibody expression in plant leaves, resulting in the production of rituximab<sup>47</sup>. Two distinct glycoengineered forms of rituximab were produced in *Nicotiana benthamiana* plants through the implementation of

different glycoengineering strategies. Briefly, the first method employed vacuum infiltration of tobacco plants with *Agrobacterium* cultures, harboring HC and LC plant expression vectors, along with 0.5  $\mu$ M kifunensine Mannosidase I Inhibitor to obtain high-mannosylated rituximab. The second approach involved the agroinfiltration of glycoengineered *N. benthamiana* plants knocked out in the  $\alpha$ (1,3)-fucosyltransferase (FucT) and  $\beta$ (1,2)-xylosyltransferase (*XylT*) genes to obtain rituximab G0<sup>48</sup>. Finally, protein A affinity chromatography was used to purify antibodies (as previously described by Tengattini and coworkers<sup>47</sup>) from agroinfiltrated kifunensine-treated and glycoengineered *N. benthamiana* plants.

### Sample preparation for MALDI-ISD MS analysis

Prior to direct infusion ESI MS, all mAbs were buffer exchanged using 30 kDa Amicon® Ultra centrifugal filters. The following amounts were processed of each mAb: 177  $\mu$ g of SiLuLite mAb, 150  $\mu$ g of Standard trastuzumab, 30  $\mu$ g of trastuzumab Man5, 90  $\mu$ g of standard rituximab, 30  $\mu$ g of rituximab G0 and 15.6  $\mu$ g of rituximab Man9. The buffer was exchanged three times by diluting the mAb with 400  $\mu$ L of 5:94.9:0.1 (v/v) ACN/H<sub>2</sub>O/TFA and centrifuging for 12 min at 8000 rpm (Eppendorf Centrifuge 5425), until ~30  $\mu$ L remained. Then, 70  $\mu$ L of 50:49.9:0.1 ACN/H<sub>2</sub>O/TFA were added and samples were infused for ESI-MS analysis. After buffer exchange, rituximab G0 and Man9 were diluted with 20  $\mu$ L of 80:19.9:0.1 ACN/H<sub>2</sub>O/TFA.

Prior to MALDI MS analysis, all mAbs were purified to remove PBS and other compounds that interfere with the MALDI-MS analysis by adapting the protocols previously described<sup>48</sup>. Briefly, 15  $\mu$ g of mAb were captured using 10  $\mu$ L of FcXL agarose beads on a 96-well filter plate. Previous to the incubation with the mAbs, the beads were washed three times with 100  $\mu$ L of 50 mM ammonium bicarbonate. Afterward, the samples diluted in 50  $\mu$ L of 50 mM ammonium bicarbonate were added to the beads and incubated on a multi-well shaker plate at 900 rpm. After the incubation step of 30 min at room temperature, the supernatant was removed and the beads were washed three times with 100  $\mu$ L of 50 mM ammonium bicarbonate and once with 100  $\mu$ L of Milli-Q H<sub>2</sub>O. Finally, the mAbs were eluted by incubation with 15  $\mu$ L of 100 mM FA on the multi-well shaker at 900 rpm for 5 min to obtain the final 1  $\mu$ g/ $\mu$ L solutions of mAbs.

### MALDI spotting

1  $\mu$ L of mAbs 1  $\mu$ g/ $\mu$ L in 100 mM FA was spotted onto an AnchorChip MALDI target plate with 1  $\mu$ L of a mixture composed of 1,5-DAN/DHB/NaHCO<sub>3</sub> 2:10:5 mM. The MALDI matrix was prepared by mixing 500 mM DHB in 9:1 (v/v) ACN/H<sub>2</sub>O, 50 mM 1,5-DAN in 1:1 (v/v) ACN/H<sub>2</sub>O and 100 mM sodium bicarbonate in H<sub>2</sub>O in a final volume of 100  $\mu$ L in 1:1 ACN/H<sub>2</sub>O. The spots were allowed to dry at room temperature, washed with cold water to remove the excess salt, and then left dry again.

All the mAbs, standard and glycoengineered were subjected to repeatability tests, from a minimum of 12 to a maximum of 14 replicates, to ensure accuracy and data consistency during quantitation.

### Direct infusion ESI, MALDI-ISD and MALDI-ISD-CID FT-ICR MS

All ESI and MALDI-ISD MS measurements were performed on a 15 T solariX 2xR FT-ICR mass spectrometer (Bruker, Bremen, Germany) equipped with a CombiSource and a ParaCell (used in xR mode) was used for the MS measurements. fmsControl software (Bruker) was used to control the MS system. Direct infusion experiments were performed using a 100  $\mu$ L syringe (Hamilton) connected by a peek tube to the ESI source, and samples were infused at 120  $\mu$ L/h using a syringe infusion pump. ESI MS spectra were acquired in the  $m/z$  range 398.18–5000 (with 128 k data points). Declustering was enhanced by setting the skimmer 1 voltage to 130 V. The number of summed scans per sample varied from 1000 to 1500. MALDI measurements were performed using a Smartbeam-II laser system (Bruker) at a frequency of 500 Hz and 200 laser shots per scan. MALDI-ISD mass spectra were acquired in the  $m/z$  range 918–5000 (with 1 M data points) and 40 scans were summed. MALDI-ISD-CID tandem mass spectra were recorded in the  $m/z$  ranges

300–8000 (with 1 M data points) and 90–8000 (with 2 M data points). CID was performed on selected precursor ions with collision energy optimized for each precursor (55–90 V).

### Bottom-up LC-MS analysis

All six mAbs were subjected to 4–12% PAGE (NuPAGE Bis-Tris Precast Gel, Life Technologies). The bands of the heavy chains were cut into four bands. Gel slices were first washed three times with water and subsequently subjected to reduction with 10 mM dithiothreitol, alkylation with 50 mM of iodoacetamide, and in-gel trypsin digestion using a Proteineer DP digestion robot (Bruker). After the addition of trypsin (at 12.5 ng/μl) and swelling of the bands, the bands were transferred to Eppendorf vials and were covered in 25 mM NH<sub>4</sub>HCO<sub>3</sub> pH 8.3. Trypsin digestion took place overnight at 37 °C and the peptides were extracted from the gel slices with 50/50/0.1 v/v/v water/acetonitrile/formic acid. Finally, peptides were lyophilized. Trypsin peptides were dissolved in water/formic acid (100/0.1 v/v) and subsequently analyzed by on-line C18 nanoHPLC MS/MS with a system consisting of an Ultimate3000nano gradient HPLC system (Thermo, Bremen, Germany), and an Exploris480 mass spectrometer (Thermo). Fractions were injected onto a cartridge precolumn (300 μm × 5 mm, C18 PepMap, 5 μm, 100 Å, and eluted via a homemade analytical nano-HPLC column (50 cm × 75 μm; Reprosil-Pur C18-AQ 1.9 μm, 120 Å (Dr. Maisch, Ammerbuch, Germany). The gradient was run from 2% to 40% solvent B (20/80/0.1 water/acetonitrile/formic acid (FA) v/v) in 30 min. The nano-HPLC column was drawn to a tip of ~10 μm and acted as the electrospray needle of the MS source. In the master scan (MS1) the resolution was 120,000, the scan range 400–3500, at standard AGC target @maximum fill time of 50 ms. A lock mass correction on the background ion of *m/z* 445.12 was used.

### Liquid-chromatography fluorescence detection

Glycan analysis of standard trastuzumab and trastuzumab Man5 by LC-FD was performed as previously reported<sup>49</sup>. Briefly, 200 μg of IgG1 were subjected to a buffer exchange (ammonium formate buffer (10 mM, pH 8.6), followed by incubation with 2 μl PNGase F (500,000 U/ml, New England BioLabs, P0705L) at 45 °C for 1 hour and 2-AB labeling at 65 °C for 2 hours with subsequent purification (in house preparation of 2AB label according to Signal 2-AB Labeling Kit, Agilent, GKK404). The labeled glycans were separated by hydrophilic interaction liquid chromatography (Acquity UPLC Glycan BEH Amide Column, 1.7 μm, 2.1 × 150 mm, Waters) with a 47.5 min gradient containing 100 mM ammonium formate, pH 4.5 (eluent A) and acetonitrile (eluent B). The fluorescence signal of the labeled glycans was detected at 420 nm (excitation wavelength at 330 nm).

### Data processing

MALDI-ISD FT-ICR mass spectra were visualized and evaluated in DataAnalysis 5.0 SR1 (Bruker). A curation of the data was performed visually, evaluating the level of the background signal. Then, a mass list was generated per mass spectrum and copied to Microsoft Excel for further processing. The signal intensities of the first three isotopic peaks of <sup>0,2</sup>A fragment ions were used to generate the glycan profiles. Theoretical fragment ions of the N-glycans were generated in GlycoWorkbench 2.1 from known glycan structures<sup>50,51</sup>. Theoretical protein fragment ions of mAbs were generated using the online tool ProteinProspector (prospector.ucsf.edu/prospector/mshome.htm). Glycopeptide LC-MS data were visualized and evaluated in Xcalibur 2.2 (Thermo). The signal intensity of glycopeptides was determined using Skyline (64 bit) 23.1.0.268 (McCoss Lab Software, University of Washington, WA, USA). Deconvolution of intact mass spectra was performed in DataAnalysis 5.0 SR1 (Bruker) using the Maximum Entropy deconvolution tool setting instrument resolving power to 5000 and resolution to “high”.

### Data availability

The numerical source data of the glycan fragment charts is provided in Supplementary Data 1. All mass spectrometry data used in this work are available from the authors upon request.

Received: 19 April 2024; Accepted: 3 September 2024;

Published online: 12 September 2024

### References

- Ebrahimi, S. B. & Samanta, D. Engineering protein-based therapeutics through structural and chemical design. *Nat. Commun.* **14**, 2411 (2023).
- Zheng, K., Bantog, C. & Bayer, R. The impact of glycosylation on monoclonal antibody conformation and stability. *mAbs* **3**, 568–576 (2011).
- Elliott, S. et al. Enhancement of therapeutic protein in vivo activities through glycoengineering. *Nat. Biotechnol.* **21**, 414–421 (2003).
- Wang, L.-X., Tong, X., Li, C., Giddens, J. P. & Li, T. Glycoengineering of Antibodies for Modulating Functions. *Annu. Rev. Biochem.* **88**, 433–459 (2019).
- Kuroguchi, M. et al. Glycoengineered Monoclonal Antibodies with Homogeneous Glycan (M3, G0, G2, and A2) Using a Chemoenzymatic Approach Have Different Affinities for FcγRIIIa and Variable Antibody-Dependent Cellular Cytotoxicity Activities. *PLoS ONE* **10**, e0132848 (2015).
- Rocamora, F. et al. Glycosylation shapes the efficacy and safety of diverse protein, gene and cell therapies. *Biotechnol. Adv.* **67**, 108206 (2023).
- Shinkawa, T. et al. The Absence of Fucose but Not the Presence of Galactose or Bisecting N-Acetylglucosamine of Human IgG1 Complex-type Oligosaccharides Shows the Critical Role of Enhancing Antibody-dependent Cellular Cytotoxicity\*. *J. Biol. Chem.* **278**, 3466–3473 (2003).
- Ferrara, C. et al. Unique carbohydrate-carbohydrate interactions are required for high affinity binding between FcγRIII and antibodies lacking core fucose. *Proc. Natl Acad. Sci. USA* **108**, 12669–12674 (2011).
- Marusic, C. et al. N-glycan engineering of a plant-produced anti-CD20-hIL-2 immunocytokine significantly enhances its effector functions. *Biotechnol. Bioeng.* **115**, 565–576 (2018).
- Luo, S. & Zhang, B. Benchmark Glycan Profile of Therapeutic Monoclonal Antibodies Produced by Mammalian Cell Expression Systems. *Pharm. Res.* **41**, 29–37 (2024).
- Shanmugaraj, B., I. Bulaon, C. J. & Phoolcharoen, W. Plant Molecular Farming: A Viable Platform for Recombinant Biopharmaceutical Production. *Plants* **9**, 842 (2020).
- Staub, J. M. et al. High-yield production of a human therapeutic protein in tobacco chloroplasts. *Nat. Biotechnol.* **18**, 333–338 (2000).
- Donini, M. & Marusic, C. Current state-of-the-art in plant-based antibody production systems. *Biotechnol. Lett.* **41**, 335–346 (2019).
- Durocher, Y. & Butler, M. Expression systems for therapeutic glycoprotein production. *Curr. Opin. Biotechnol.* **20**, 700–707 (2009).
- Huang, W., Giddens, J., Fan, S.-Q., Toonstra, C. & Wang, L.-X. Chemoenzymatic Glycoengineering of Intact IgG Antibodies for Gain of Functions. *J. Am. Chem. Soc.* **134**, 12308–12318 (2012).
- Zhang, L., Luo, S. & Zhang, B. Glycan analysis of therapeutic glycoproteins. *mAbs* **8**, 205–215 (2016).
- Reusch, D. et al. Comparison of methods for the analysis of therapeutic immunoglobulin G Fc-glycosylation profiles—Part 1: Separation-based methods. *mAbs* **7**, 167–179 (2015).
- Szrenti, K. et al. Interlaboratory Study for Characterizing Monoclonal Antibodies by Top-Down and Middle-Down Mass Spectrometry. *J. Am. Soc. Mass Spectrom.* **31**, 1783–1802 (2020).
- Qu, M. et al. Qualitative and quantitative characterization of protein biotherapeutics with liquid chromatography mass spectrometry. *Mass Spectrom. Rev.* **36**, 734–754 (2017).
- Reusch, D. et al. Comparison of methods for the analysis of therapeutic immunoglobulin G Fc-glycosylation profiles—Part 2: Mass spectrometric methods. *mAbs* **7**, 732–742 (2015).

21. Tran, B. Q. et al. Comprehensive glycosylation profiling of IgG and IgG-fusion proteins by top-down MS with multiple fragmentation techniques. *J. Proteom.* **134**, 93–101 (2016).
22. Tran, B. Q. et al. Glycosylation characterization of therapeutic mAbs by top- and middle-down mass spectrometry. *Data Brief.* **6**, 68–76 (2016).
23. van der Burgt, Y. E. M. et al. Structural Analysis of Monoclonal Antibodies by Ultrahigh Resolution MALDI In-Source Decay FT-ICR Mass Spectrometry. *Anal. Chem.* **91**, 2079–2085 (2019).
24. Mojumdar, A. et al. Advances in mass spectrometry-based approaches for characterizing monoclonal antibodies: resolving structural complexity and analytical challenges. *J. Anal. Sci. Technol.* **15**, 23 (2024).
25. Jin, Y. et al. Comprehensive characterization of monoclonal antibody by Fourier transform ion cyclotron resonance mass spectrometry. *mAbs* **11**, 106–115 (2019).
26. Zhu, W., Li, M. & Zhang, J. Integrating Intact Mass Analysis and Middle-Down Mass Spectrometry Approaches to Effectively Characterize Trastuzumab and Adalimumab Structural Heterogeneity. *J. Proteome Res.* **20**, 270–278 (2021).
27. Harvey, D. J. Analysis of carbohydrates and glycoconjugates by matrix-assisted laser desorption/ionization mass spectrometry: An update for 2019–2020. *Mass Spectrom. Rev.* **42**, 1984–2206 (2023).
28. Selman, M. H. J., Hemayatkar, M., Deelder, A. M. & Wührer, M. Cotton HILIC SPE Microtips for Microscale Purification and Enrichment of Glycans and Glycopeptides. *Anal. Chem.* **83**, 2492–2499 (2011).
29. Murray, D. L. et al. Mass spectrometry for the evaluation of monoclonal proteins in multiple myeloma and related disorders: an International Myeloma Working Group Mass Spectrometry Committee Report. *Blood Cancer J.* **11**, 24 (2021).
30. Resemann, A. et al. Full validation of therapeutic antibody sequences by middle-up mass measurements and middle-down protein sequencing. *mAbs* **8**, 318–330 (2016).
31. Gstöttner, C. et al. Monitoring glycation levels of a bispecific monoclonal antibody at subunit level by ultrahigh-resolution MALDI FT-ICR mass spectrometry. *mAbs* **12**, 1682403 (2020).
32. Tyshchuk, O. et al. Characterization and prediction of positional 4-hydroxyproline and sulfotyrosine, two post-translational modifications that can occur at substantial levels in CHO cells-expressed biotherapeutics. *mAbs* **11**, 1219–1232 (2019).
33. Köcher, T., Engström, Å. & Zubarev, R. A. Fragmentation of Peptides in MALDI In-Source Decay Mediated by Hydrogen Radicals. *Anal. Chem.* **77**, 172–177 (2005).
34. Hardouin, J. Protein sequence information by matrix-assisted laser desorption/ionization in-source decay mass spectrometry. *Mass Spectrom. Rev.* **26**, 672–682 (2007).
35. Fukuyama, Y., Iwamoto, S. & Tanaka, K. Rapid sequencing and disulfide mapping of peptides containing disulfide bonds by using 1,5-diaminonaphthalene as a reductive matrix. *J. Mass Spectrom.* **41**, 191–201 (2006).
36. Asakawa, D., Calligaris, D., Zimmerman, T. A. & Pauw, E. D. In-Source Decay during Matrix-Assisted Laser Desorption/Ionization Combined with the Collisional Process in an FTICR Mass Spectrometer. *Anal. Chem.* **85**, 7809–7817 (2013).
37. Nicolardi, S., Switzar, L., Deelder, A. M., Palmblad, M. & van der Burgt, Y. E. M. Top-Down MALDI-In-Source Decay-FTICR Mass Spectrometry of Isotopically Resolved Proteins. *Anal. Chem.* **87**, 3429–3437 (2015).
38. Nicolardi, S. et al. Evaluation of Sibling and Twin Fragment Ions Improves the Structural Characterization of Proteins by Top-Down MALDI In-Source Decay Mass Spectrometry. *Anal. Chem.* **92**, 5871–5881 (2020).
39. Urakami, S. & Hinou, H. Direct MALDI Glycotyping of Glycoproteins toward Practical Subtyping of Biological Samples. *ACS Omega* **7**, 39280–39286 (2022).
40. Urakami, S. & Hinou, H. Glycan-Selective MALDI In-Source Decay Analysis of Intact Glycoproteins. *Anal. Sens.* **2**, e202100040 (2022).
41. Nicolardi, S. et al. Glycan and Protein Analysis of Glycoengineered Bacterial *E. coli* Vaccines by MALDI-in-Source Decay FT-ICR Mass Spectrometry. *Anal. Chem.* **94**, 4979–4987 (2022).
42. Hudis, Clifford A. Trastuzumab — Mechanism of Action and Use in Clinical Practice. *N. Engl. J. Med.* **357**, 39–51 (2007).
43. Pescovitz, M. D. Rituximab, an Anti-CD20 Monoclonal Antibody: History and Mechanism of Action. *Am. J. Transplant.* **6**, 859–866 (2006).
44. Jansing, J., Sack, M., Augustine, S. M., Fischer, R. & Bortesi, L. CRISPR/Cas9-mediated knockout of six glycosyltransferase genes in *Nicotiana benthamiana* for the production of recombinant proteins lacking  $\beta$ -1,2-xylose and core  $\alpha$ -1,3-fucose. *Plant Biotechnol. J.* **17**, 350–361 (2019).
45. de Haan, N. et al. Linkage-specific sialic acid derivatization for MALDI-TOF-MS profiling of IgG glycopeptides. *Anal. Chem.* **87**, 8284–8291 (2015).
46. Wührer, M., Koeleman, C. A. M., Hokke, C. H. & Deelder, A. M. Mass spectrometry of proton adducts of fucosylated N-glycans: fucose transfer between antennae gives rise to misleading fragments. *Rapid Commun. Mass Spectrom.* **20**, 1747–1754 (2006).
47. Tengattini, S. et al. Multi-approach LC-MS methods for the characterization of species-specific attributes of monoclonal antibodies from plants. *J. Pharm. Biomed. Anal.* **216**, 114796 (2022).
48. Blöchl, C. et al. A robust nanoscale RP HPLC-MS approach for sensitive Fc proteoform profiling of IgG allotypes. *Analytica Chim. Acta* **1279**, 341795 (2023).
49. Thomann, M. et al. In Vitro Glycoengineering of IgG1 and Its Effect on Fc Receptor Binding and ADCC Activity. *PLoS ONE* **10**, e0134949 (2015).
50. Ceroni, A. et al. GlycoWorkbench: A Tool for the Computer-Assisted Annotation of Mass Spectra of Glycans. *J. Proteome Res.* **7**, 1650–1659 (2008).
51. Damerell, D. et al. The GlycanBuilder and GlycoWorkbench glycoinformatics tools: updates and new developments. *Biol. Chem.* **393**, 1357–1362 (2012).

## Acknowledgements

We acknowledge the financial support provided by the University of Pavia and the Erasmus Traineeship programme that enabled Isabella Senini (University of Pavia) to reside in the Netherlands and contribute to the study. Additionally, gratitude is extended to Roche Diagnostics GmbH (Germany), ENEA Casaccia Research Center (Italy) for providing the glycoengineered mAbs and Julia Jansing and Luisa Bortesi for kindly providing *N. benthamiana* FX-KO seeds from RWTH Aachen University.

## Author contributions

S.N. devised the conceptual idea and supervised the project. M.W. helped supervise the project. D.R., C.M. and M.D. manufactured the samples. I.S. designed and performed experiments. S.T. and F.R. preliminary characterized the samples. I.S. and S.N. processed the experimental data, designed the figures, and drafted the manuscript. P.A.V.V. contributed to sample analysis. G.M., M.W., C.T., E.D.V., C.G., S.T., and F.R. provided critical feedback and helped shape the research and manuscript. All authors reviewed the manuscript.

## Competing interests

The authors declare no competing interests.

### Additional information

**Supplementary information** The online version contains supplementary material available at <https://doi.org/10.1038/s42004-024-01297-x>.

**Correspondence** and requests for materials should be addressed to Simone Nicolardi.

**Peer review information** *Communications Chemistry* thanks Hiroshi Hinou, Stephanie Archer-Hartmann, and the other, anonymous, reviewer for their contribution to the peer review of this work.

**Reprints and permissions information** is available at <http://www.nature.com/reprints>

**Publisher's note** Springer Nature remains neutral with regard to jurisdictional claims in published maps and institutional affiliations.

**Open Access** This article is licensed under a Creative Commons Attribution-NonCommercial-NoDerivatives 4.0 International License, which permits any non-commercial use, sharing, distribution and reproduction in any medium or format, as long as you give appropriate credit to the original author(s) and the source, provide a link to the Creative Commons licence, and indicate if you modified the licensed material. You do not have permission under this licence to share adapted material derived from this article or parts of it. The images or other third party material in this article are included in the article's Creative Commons licence, unless indicated otherwise in a credit line to the material. If material is not included in the article's Creative Commons licence and your intended use is not permitted by statutory regulation or exceeds the permitted use, you will need to obtain permission directly from the copyright holder. To view a copy of this licence, visit <http://creativecommons.org/licenses/by-nc-nd/4.0/>.

© The Author(s) 2024